Acta Cryst. (1966). **21**, 629

The Precession Method in Fiber Diffraction Photography

By Murray Vernon King
Department of Orthopedic Surgery, The Harvard Medical School, Massachusetts General Hospital, Boston, Massachusetts 02114, *U.S.A.*

(*Received* 12 *April* 1965)

The precession method is recommended for taking diffraction patterns of highly-ordered fiber specimens in cases where the theoretical advantages of recording an undistorted meridional slice of the Fourier transform of the specimen are called for by the nature of the research problem, *e.g.* when the diatropic (meridional) reflections are of especial interest. Analysis of the process of image formation shows that the fidelity of recording the transform is limited by the width of the layer-line slit. The resulting resolution of the Fourier transform in reciprocal space is approximately $2(\Delta r/r)\sin^2\bar{\mu}$, where r is the radius and Δr the half-width of the slit. Use of a narrower slit to improve the resolution entails a correspondingly longer exposure. Experimental data, mostly on chitin, illustrate these features, and show that the exposure times required for the sharpest patterns may range to more than forty times those required in the usual diffraction method employing a stationary specimen.

Introduction

The goal of the investigation of any fiber by X-ray diffraction is to record the Fourier transform of the fiber. More specifically, the entity recorded is the Fourier transform of the electron-density function of the real fiber as influenced by such factors as disorientation and other disorders, rather than the transform of the ideal unit cell.

The choice of the diffraction method to apply depends fundamentally on a compromise between fidelity and convenience afforded by the various methods in achieving this goal. Howsmon & Walter (1960) have suggested the application of the Buerger precession camera for recording the diffraction patterns of fibers, citing the following advantages:

(*a*) An undistorted slice of the Fourier transform is recorded on the film.

(*b*) The diatropic (meridional) reflections are included, whereas they lie outside the region theoretically recordable when one applies the most usual technique of taking the diffraction pattern of a stationary specimen with the X-ray beam normal to the fiber axis.

This article will discuss some relative advantages and disadvantages of the precession method, especially in terms of specimen quality, resolution in the recorded pattern, and exposure time, and the results of experiments illustrating these points will be described.

Definitions and assumptions

It will be assumed, unless stated otherwise, that the fiber specimen is mounted with its axis along the spindle axis of the precession camera. Thus, this axis is horizontal on the resultant photographs. Stationary photographs taken in the precession camera will naturally have the same orientation, whereas this axis is set vertical in the usual fiber cameras. Whatever the orientation of the specimen in laboratory space, the direction of the fiber axis will be termed the 'meridional' direction and the normal to it will be termed 'equatorial'.

We shall also assume, unless stated otherwise, that precession photographs are taken with the settings of the film and layer-line screen calculated for zero-layer photography.

In characterizing a fiber specimen, we must specify the type of orientation (uniaxial, biaxial, *etc.*) and the perfection with which this orientation is maintained. The Fourier transform of a normal uniaxial fiber is cylindrically symmetric about the fiber axis, and thus the recording of a single meridional section of the transform (*i.e.* a section containing the fiber axis) serves to characterize the entire transform. On the other hand, a biaxial (doubly-oriented) fiber has a Fourier transform defined in three dimensions, which must be recorded by methods resembling those applied to single crystals.

Image formation of continuous Fourier transforms in the precession camera

In recording diffraction patterns of single crystals, the diffracting power is largely limited to discrete points (Bragg spots) or lines (white radiation streaks). Only a background of diffuse scattering fills the rest of reciprocal space. Thus the width of the slit in the layer-line screen is an important factor only in isolating layers from their neighbors and in reducing the diffuse background. In contrast, in fiber diffractometry the crystallite sizes are generally small enough, or the disorder sufficient, that the Fourier transform covers extended regions of reciprocal space. Thus, when one takes a zero-layer film in an effort to obtain a meridional section of the Fourier transform, the finite slit width permits a nest of coaxial cones of diffracted radiation of differing angles $\bar{\nu}$ to pass. Each cone corresponds to a reciprocal lattice plane parallel to the film. Thus, an entire slab of reciprocal space is simultaneously recorded on the film.

Other factors limiting the resolution involve beam convergence, which is a function of the sizes of the focal spot and the specimen, or of the collimator system. However, we shall neglect these factors here, assuming that the conditions have been chosen so that they do not become the limiting factors.

We shall elucidate the nature of the image produced on the film under the stated conditions, and determine how it is influenced by the aberrations inherent in the precession method and by the slit width adopted in a given experiment.

The imaging process has the following features:

(1) Each point in the zero plane of the Fourier transform produces a single image in its correct place on the film, just as in the single-crystal case. However, here we must define 'zero plane' to mean the central plane of the Fourier transform lying parallel to the film, without reference to a reciprocal lattice.

(2) Points lying outside the zero plane give double images, displaced from the positions that the points occupy in their respective planes. Thus, features lying in planes parallel to the zero plane will be represented on the film as distorted double images overlapping the image of the zero plane. As is often done in precession theory, we can alternatively treat the points outside the zero plane as being imaged on the film, or *on the zero plane*. The latter procedure allows us to treat the object and image as though both existed in the same reciprocal space.

(3) The geometry of the image of any point or extended feature in reciprocal space is determined only by the precession motion, *i.e.* orientation of the precession axis and precession angle $\bar{\mu}$.

(4) The layer-line screen acts only by selecting which planes are permitted to record, without affecting the aberrations present in their images.

(5) Owing to the overlap of images arising from different reciprocal-lattice planes, the image formation is a many-to-one process. We shall define the anti-image of a point or extended feature on the film (or on the zero plane) as being the locus of all points in reciprocal space contributing to the given image. The anti-image of a point will be seen to be a space curve, that of a line is a curved surface, and the anti-image of an extended area is a solid figure.

While the analytical calculation of the positions of image points in the precession method is cumbersome, the geometric constructions shown by Buerger (1944, 1964) provide a simple graphical means of constructing both images and anti-images. The diagrams presented in this article to illustrate these features have been so constructed. The analogous and geometrically identical problem for the retigraph has been treated by Mackay (1960).

Fig. 1 depicts the anti-image of a point I in the zero plane. We assume that no layer-line screen is used, and adopt a frame of reference in which the specimen is fixed, while the sphere of reflection is made to precess about the normal to the zero plane (the ζ axis). The successive positions of the incident beam vector are thus unit vectors constituting elements of the cone COC'. During the precession cycle, the diffracted beams contributing to the image at I will arise from successive positions CC' of the center of the sphere of reflection. Thus they lie along the elements of the oblique circular cone CIC'. The diffracted-beam vectors CA are of unit length. This establishes the anti-image AIA' as being the curve on the surface of the oblique circular cone cutting the elements of the cone at unit distance above the base. Fig. 2 shows the relation of the anti-image to the zero plane, with its orthogonal projection in that plane sketched in for reference.

Some images of specific figures in reciprocal space

The images of nets in planes parallel to the zero plane are of interest in illustrating the magnitude and direction of the aberrations inherent in the zero-layer film.

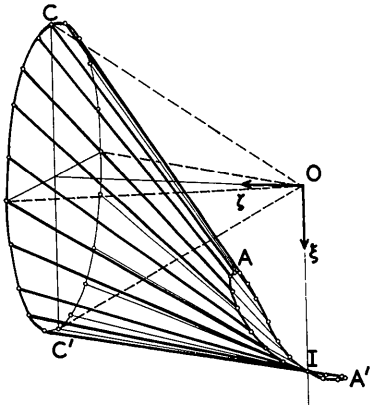

Fig. 1. Construction of the anti-image curve AIA' of the image point I in the zero plane. The origin of reciprocal space is at O. The center of the sphere of reflection traverses the circle CC' during the precession motion.

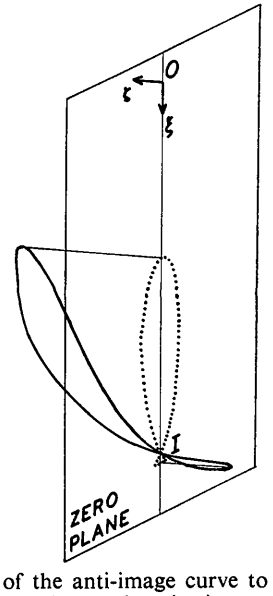

Fig. 2. Relation of the anti-image curve to the zero plane as shown by orthogonal projection on the latter.

Fig. 3 shows this for the case of a net of spacing 0·4 reciprocal-lattice units, situated at $\zeta = 0{\cdot}2$. At the left and center, a portion of the recordable region of this layer is shown in undistorted form. Overlaying it is the right-hand half of the precession image of the net on the zero plane. The image points of the latter are connected in such a way as to reveal the two component nets with their complementary distortions. The drawing is constructed for $\bar{\mu} = 30°$.

The image of a spherical surface about the origin is of practical interest for several reasons. First, a powder line (*e.g.* due to an included mineral) is the equivalent of such a sphere in reciprocal space. Further, features in the Fourier transform broadened by partial disorientation are spread out over portions of spherical surfaces (namely zones, if the overall orientation is uniaxial). Fig. 4 shows a portion of the image of a spherical surface of radius 0·5 (again, $\bar{\mu} = 30°$). The equator of the sphere is taken in the zero plane, and the images of several meridians and parallels are shown. A portion of the map of the Western Hemisphere is sketched in to aid in visualizing the aberrations. The following characteristics of such images must be taken into account in order to avoid false interpretation of the corresponding features on precession films:

(1) Let ϱ be the radius of the sphere, and $\theta = \sin^{-1}(\varrho/2)$. Then, only the zone of the spherical surface lying between $\zeta = \varrho \sin(\theta \pm \bar{\mu})$ can be recorded. The corresponding image covers an annulus lying in the range between $\xi = \sin 2\theta / \cos(\bar{\mu} \pm 2\theta)$. Thus, in Fig. 4, the zone from $\zeta = -0{\cdot}134$ to $+0{\cdot}350$ is recorded as an annulus from $\xi = 0{\cdot}484$ to $0{\cdot}938$.

(2) If we assume that the Fourier transform has a constant density distributed over the spherical surface, then the image will be shaded most densely at its inner margin, owing to the crowding of image points there. The illusion of a 'line' is thus created. In general, this 'line' will not be situated at the correct radius ϱ, except when $\theta = \bar{\mu}$.

(3) When we insert a layer-line screen, we limit the image to a narrower annulus on the film, but only in the limiting case of an infinitely narrow slit will the inner margin of the image always occur at $\xi = \varrho$.

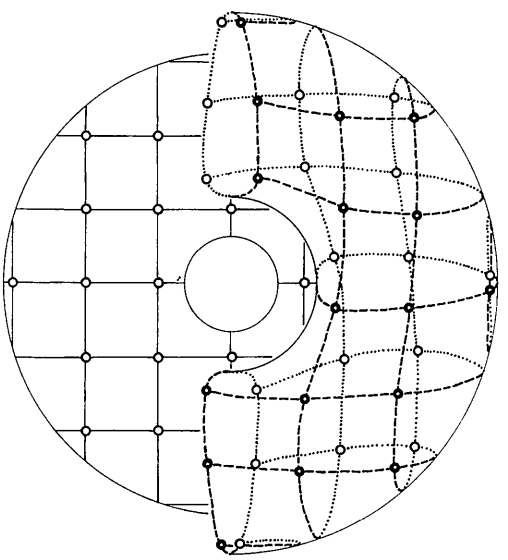

Fig. 3. The relation of a net in a non-zero plane to its precession image on the zero plane. Left and center: part of the recordable region of a net of spacing 0·4 reciprocal-lattice units lying in the plane at $\zeta = 0{\cdot}2$. Right: half of its precession image.

Resolution of the precession image

Now we can consider the 'resolution' afforded by the precession method. By this term, which we can inter-

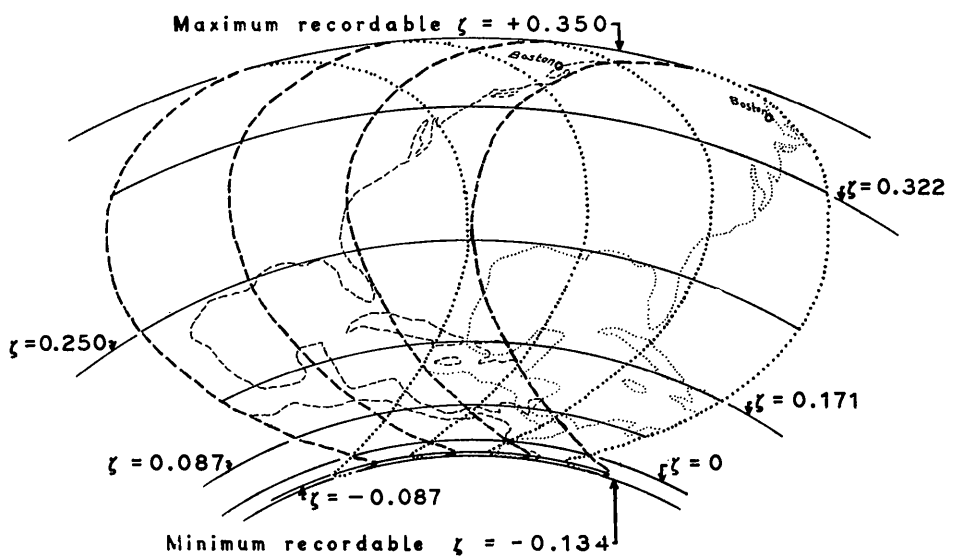

Fig. 4. The precession image of a 30° sector of a sphere of radius 0·5 reciprocal lattice units centered at the origin of reciprocal space. Precession angle $\bar{\mu} = 30°$. The equator of the sphere is taken in the zero plane, and the images of meridians and parallels at intervals of 10° are drawn in. Part of the map of the Western Hemisphere is sketched in to aid in visualizing the aberrations and the limits of the recordable region of the spherical surface.

pret as a 'distance of confusion' in the Fourier transform, we mean the maximum span covered in reciprocal space by points that will contribute to the image at a given point on the film, and thus be confused in the precession pattern.

Fig. 5 shows the portion of the anti-image of the point I which is permitted to contribute to the image at I when a layer-line screen is inserted. Here ζ_+ is the coordinate of the reciprocal-lattice plane corresponding to the maximum cone angle $\bar{\nu}_+$ permitted to record, and ζ_- similarly corresponds to the minimum angle $\bar{\nu}_-$. The values δ_+ and δ_- are the linear distances from the image point I to the intercepts of the anti-image curve in the ζ_+ and ζ_- planes, respectively. While the intercept points are not exactly collinear with I, the total maximum distance between the intercept points is well approximated by

$$\delta_\pm = |\delta_+| + |\delta_-| \,. \tag{1}$$

The value of $\delta_\pm$ is a measure of the 'resolution' obtainable under the given conditions.

Now let us assume that the slit of radius r and half-width Δr is properly set to record the zero layer. (Here Δr is actually one-half the width unobscured by the screen, a quantity varying with the cone angle.)

Then, following Buerger [1964, p.68, equation (3)] and setting $n=0$ and $s=r \cot \bar{\mu}$, we have

$$\Delta r = (r \cot \bar{\mu}) \tan [\cos^{-1}(\cos \bar{\mu} - \zeta_+)] - r \,. \tag{2}$$

Solving for ζ_+, we have

$$\zeta_+ = \cos \bar{\mu} - [1 + \tan^2 \bar{\mu}(1 + \Delta r/r)^2]^{-\frac{1}{2}} \,. \tag{3}$$

Similarly,

$$\zeta_- = \cos \bar{\mu} - [1 + \tan^2 \bar{\mu}(1 - \Delta r/r)^2]^{-\frac{1}{2}} \,. \tag{4}$$

For small values of $\Delta r/r$, these expressions may be approximated by

$$\zeta_+ = \sin^2 \bar{\mu} \cos \bar{\mu}(\Delta r/r) \,, \tag{5}$$

$$\zeta_- = -\sin^2 \bar{\mu} \cos \bar{\mu}(\Delta r/r) \,.$$

Now the intercept points of the anti-image curve in the ζ_+ plane are both displaced in the ζ direction from the image point I by the distance ζ_+, and normal to this by $\zeta_+ \tan \bar{\nu}_+$ (where $\cos \bar{\nu}_+ = \cos \bar{\mu} - \zeta_+$). Thus, their total displacement δ_+ in reciprocal space is given by

$$\delta_+ = \zeta_+ \sec \bar{\nu}_+ = \zeta_+/(\cos \bar{\mu} - \zeta_+) \,. \tag{7}$$

Similarly, the intercepts in the ζ_- plane are displaced from the image point by

$$\delta_- = \zeta_- \sec \bar{\nu}_- = \zeta_-/(\cos \bar{\mu} - \zeta_-) \,. \tag{8}$$

For small values of $\Delta r/r$, the corresponding approximations are:

$$\delta_+ = (\Delta r/r) \sin^2 \bar{\mu} \,, \tag{9}$$

$$\delta_- = -(\Delta r/r) \sin^2 \bar{\mu} \,. \tag{10}$$

Fig. 6 shows the variation of the values of ζ_+ and ζ_- and δ_+ and δ_- as functions of $\Delta r/r$.

Thus, in the general case we can approximate the overall 'resolution' or 'distance of confusion' by the formula

$$\delta_\pm = \zeta_+/(\cos \bar{\mu} - \zeta_+) - \zeta_-/(\cos \bar{\mu} - \zeta_-) \,, \tag{11}$$

or for small $\Delta r/r$,

$$\delta_\pm = 2(\Delta r/r) \sin^2 \bar{\mu} \,. \tag{12}$$

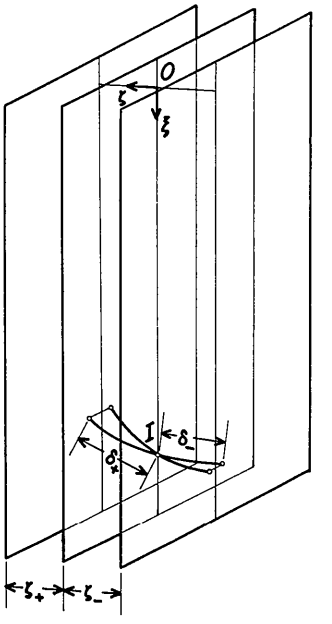

Fig. 5. Diagram of the portion of the anti-image curve permitted to contribute to the image at I when a layer-line screen is inserted.

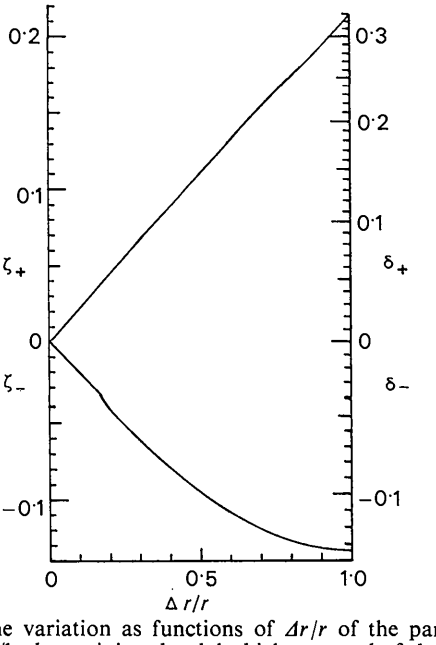

Fig. 6. The variation as functions of $\Delta r/r$ of the parameters ζ_+ and ζ_- determining the slab thickness, and of the parameters δ_+ and δ_- determining the distances to the most remote points of the Fourier transform confused in the precession image. $\bar{\mu}=30°$.

These expressions give an approximation for the limiting resolution of features of the Fourier transform in reciprocal space obtainable with the given slit width. We can convert them to corresponding expressions for the 'resolution' in real space, namely, $\lambda/\delta_{\pm}$. Note that this quantity is *not* the same as the resolution commonly quoted in single-crystal studies, since it is a measure of the longest spacings that can be discerned, rather than the shortest. For small $\Delta r/r$, the expression for the real-space 'resolution' is

$$\lambda/\delta_{\pm}=\lambda/[2(\Delta r/r)\sin^2\bar{\mu}]\,. \qquad (13)$$

Calculation shows that equation (13) is quite adequate for use with any of the layer-line screens normally used with the precession camera. Further, we note that the limiting resolution attainable with the usual slit of 5 mm is quite modest. Thus, for the commonly-supplied screen of radius $r=15$ mm, halfwidth $\Delta r=2{\cdot}5$ mm, when operating at $\bar{\mu}=30°$, $\lambda=1{\cdot}5418$ Å, we calculate a limiting resolution $\lambda/\delta_{\pm}$ of only 18·5 Å. This indicates that considerably narrower slits will be required for the sharpest resolution of detail, with a concomitant increase in the exposure time proportional to $1/\Delta r$. For example, a screen which we have used, having $r=14$ mm, $\Delta r=0{\cdot}5$ mm, should give a limiting resolution of 86 Å under these conditions, with five times the exposure to get comparable blackening.

Thus, as long as we are dealing with a continuous Fourier transform, the precession method is inherently limited in its resolution in reciprocal space by the factor of prohibitive exposure times. Only under special conditions can we resolve finer detail, as when the transform is closely limited to sharp successive maxima along the meridian. However, such conditions are more analogous to the case of a single crystal, for which we can obtain much higher 'resolutions' in the precession method by virtue of the fact that the Fourier transform is essentially zero throughout most of reciprocal space.

Experimental

Diffraction patterns were taken of a set of fiber specimens to give a concrete picture of the pertinence of the discussed factors to the overall usefulness of the precession method in fiber diffractometry.

A chitin specimen was chosen for the fullest study. This sample was lobster apodeme demineralized with ethylenediaminetetra-acetic acid, washed, and dried. Two precession patterns taken 90° apart normal to the fiber axis showed some difference in sharpness, indicating that the degree of orientation was not cylindrically symmetric about the axis. Since the pattern taken with the zero plane perpendicular to the plane of flattening of the specimen was sharper, this orientation was adopted for the remainder of the exposures.

The photographs to be compared were examined for sharpness and relative intensities of the different reflections, with particular account of how well the diatropic reflections were made manifest. Selected photographs were characterized quantitatively by scanning them along the meridian with a Joyce-Loebl microdensitometer equipped with a wedge having an absorbance range 0–2. The densitometer scans are presented here, rather than the original photographs, since experience has shown the fidelity of half-tone printing as applied to diffraction patterns to be so limited that the printed reproductions might well support erroneous conclusions diametrically opposite to those drawn from examination of the originals. The patterns of interest are:

Fig. 7. Stationary photograph, $\bar{\mu}=0°$, 5·0 hr exposure.

Fig. 8. Precession photograph, $\bar{\mu}=30°$, no layer-line screen, 5·0 hr exposure.

Fig. 9. Precession photograph, $\bar{\mu}=30°$, $r=15$ mm, $\Delta r=2{\cdot}5$ mm, 42·6 hr exposure.

Fig. 10. Precession photograph, $\bar{\mu}=30°$, $r=14$ mm, $\Delta r=0{\cdot}5$ mm, 213·2 hr exposure.

The success of the precession method in recording diatropic reflections is shown by the 060 reflection visible at the extreme left of Figs. 9 and 10, but absent in Fig. 7. The 040 diatropic reflection is also greatly strengthened in the precession patterns. Fig. 10 shows a gain in sharpness over Fig. 9, at the cost of a much longer exposure, indicating that the broader slit does not exhaust the resolution available in the Fourier transform of the specimen. However, no essentially new features are revealed by the use of the narrower slit. The spacing calculated for the 060 reflection, as calculated from the positions measured on the photographs, is 1·726 Å (5 mm slit), or 1·713 Å (1 mm slit), as compared with the value 1·71 Å reported by Carlström (1957).

Now, the use of the precession method without a layer-line screen would seem to combine the favorable features of recording the diatropic reflections, while permitting the short exposures that suffice in the stationary normal-beam method. Fig. 8 shows the result of taking the pattern under these conditions. The inherent loss of resolution is found to defeat these aims. While the 060 point in the Fourier transform is brought into diffracting position under this procedure, no corresponding peak appears on the photograph. Evidently, the weak diffraction peak produced at this short exposure is completely hidden in the surrounding continuous background. The lower-order peaks in this photograph show a characteristic appearance in having inner margins much sharper than their outer margins. Also, the peaks are displaced inward from the positions of the corresponding peaks in the precession patterns taken with layer-line screens. These two facts recall the predicted character of the image of a spherical surface, in which the image points are crowded toward an inner margin not coinciding in radius with the sphere itself.

Precession and stationary photographs were taken from a set of other fibers, which proved to be less

well oriented, and here the precession patterns proved to be hardly different from the stationary patterns. The fibers were collagen (kangaroo and rat tail tendons) and α-keratin (cat claw). No essentially new features were observed, but collagen showed sharpening and enhancement of the 2·9 Å meridional arc on the precession films. The characteristic 1·47 Å diatropic reflection of α-keratin was not recorded, being outside the range attainable with CuKα radiation at $\bar{\mu}=30°$. (However, the cat-claw specimen gives a weak 1·47 Å reflection when examined in the Weissenberg camera with the same radiation.)

Discussion and conclusions

The experimental results confirm the expectations that the precession method should be effective in recording the diatropic reflections and in permitting undistorted measurement of the positions in reciprocal space of observed features. At the same time, high resolution is gained only at the cost of enormous exposure times. The procedure of taking precession photographs without a layer-line screen has proved to lack merit, since the superposition of images arising from an extended volume of reciprocal space blurs and distorts details greatly. We might note that the oscillation method shares the same shortcoming, with the added defect that one cannot conveniently use a layer-line screen in this method.

The decision whether the precession method offers significant advantages in a given problem will depend on the nature of the specimen and the type of information we intend to get from it. The following considerations may be helpful:

(1) The precession method is worthwhile only with highly ordered specimens. Poorer specimens are, in a sense, self-precessing.

(2) Interest in the positions and intensities of the diatropic reflections favors the use of the precession method. For example, it may prove valuable in distinguishing between strictly diatropic and slightly off-axis reflections.

(3) The precession method can give an undistorted picture of the degree and type of orientation of a specimen. For example, two precession patterns taken with settings 90° apart on the spindle axis can give a good unbiased estimate of the extent of biaxial orientation of a specimen.

The author wishes to thank Mrs Muriel H. Blanchard and Dr Laurence C. Bonar for sample preparations, and Mr Syed A. Rizvi for assistance in densitometry. Specimens were supplied by Dr Alexander Rich and from the laboratory of Dr Winfield S. Morgan. The author also wishes to commend the patience of Mishka*, who graciously supplied the keratin specimen.

* Deceased 23 March 1966.

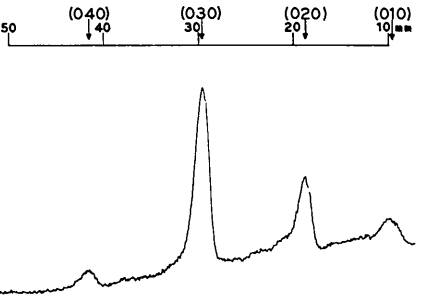

Fig. 7. Densitometer scan along meridian of stationary photograph, lobster apodeme, $\bar{\mu}=0°$, 5·0 hr. exposure. A scale of distances from the center of the film and the indices of the visible features are given.

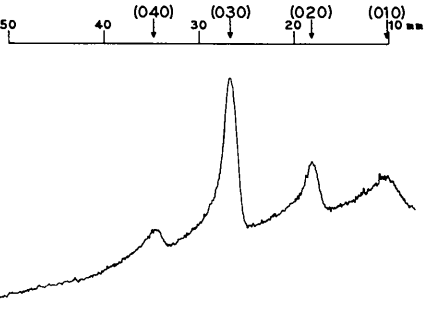

Fig. 8. Densitometer scan along meridian of precession photograph, lobster apodeme, $\bar{\mu}=30°$, no layer-line screen, 5·0 hr exposure.

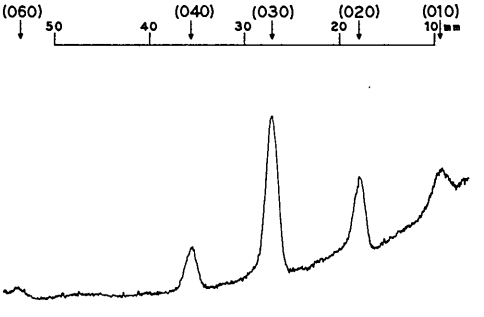

Fig. 9. Densitometer scan along meridian of precession photograph, lobster apodeme, $\bar{\mu}=30°$, $r=15$ mm, $\Delta r=2·5$ mm, 42·6 hr exposure.

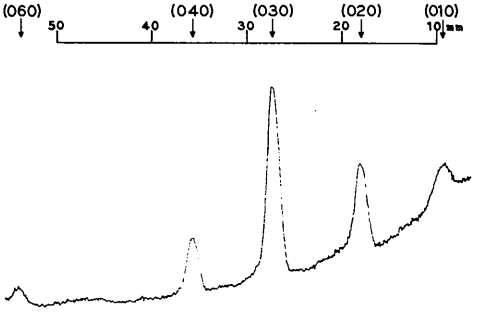

Fig. 10. Densitometer scan along meridian of precession photograph, lobster apodeme, $\bar{\mu}=30°$, $r=14$ mm, $\Delta r=$ 0·5 mm, 213·2 hr exposure.

This work has been supported by grants from the U.S. Health Service (Nos. AM-04852, DE-01777, and AM-06375) and the John A. Hartford Foundation, Inc.

References

BUERGER, M. J. (1944). *The Photography of the Reciprocal Lattice*. Monograph No. 1, American Society for X-Ray and Electron Diffraction.

BUERGER, M. J. (1964). *The Precession Method in X-Ray Crystallography*. New York: John Wiley.

CARLSTRÖM, D. (1957). *J. Biophys. Biochem. Cytol.* **3**, 669.

HOWSMON, J. A. & WALTER, N. M. (1960). In *Physical Methods in Chemical Analysis*. Ed. W. G. Berl. 2nd Edition, Vol. I, pp. 129–183 (see especially pp. 154, 161). New York: Academic Press.

MACKAY, A. L. (1960). *Acta Cryst.* **13**, 240.

Acta Cryst. (1966). **21**, 635

Measurements of the Thermal Variation of the X-ray Debye Temperature of Pure Nickel and Chromium* †

BY RONALD H. WILSON ‡, EARL F. SKELTON § AND J. LAWRENCE KATZ

X-ray Laboratory, Department of Physics, Rensselaer Polytechnic Institute, Troy, New York, U.S.A.

(*Received* 14 *March* 1966 *and in revised form* 9 *May* 1966)

The X-ray Debye temperature has been determined from integrated X-ray intensity data for single crystals of nickel and chromium in the temperature range $100°K < T < 520°K$. The data were corrected for thermal diffuse scattering as well as changes in the lattice parameters. The room temperature values of the Debye temperature were found to be $410° \pm 10°K$ and $545° \pm 20°K$ for nickel and chromium, respectively. This is in agreement with already published values for nickel; chromium, however, appears to give a room temperature Debye temperature which is somewhat lower than has been previously reported.

In the case of both metals, the elastic constant Debye temperature was computed from the available elastic constant data. In both cases, the elastic constant Debye temperature, Θ_E, was found to be greater than the X-ray Debye temperature, Θ_M. This is in agreement with previously reported values for nickel; in contradiction to published results, however, chromium was found to conform to the general relation that $\Theta_E/\Theta_M > 1$.

Introduction

Debye temperatures are frequently used to characterize the thermal vibrations of a solid and are found to be useful parameters in a number of physical properties of solids. Herbstein (1961) has recently reviewed the methods of measuring Debye temperatures and has discussed the reasons for the different values obtained from different physical measurements.

One means for determining the Debye temperature is through studying the intensity of a Bragg reflection in X-ray diffraction. The integrated Bragg intensities have been measured over a wide temperature range. From these intensity measurements, the thermal variation of the Debye temperature has been obtained.

* This work was supported in part by the National Aeronautics and Space Administration through the Rensselaer Polytechnic Institute Interdisciplinary Materials Research Center, the National Institute of Dental Research under Grant 5T1 DE117-02 and the Army Research Office (Durham).

† A portion of this study was extracted from a thesis submitted by one of the authors (R.H.W.) to the Graduate School of Rensselaer Polytechnic Institute in partial fulfillment of the requirements for the degree of Doctor of Philosophy in the Department of Physics.

‡ Present address: General Electric Research Laboratory, Schenectady, New York.

§ N.I.D.R. Predoctoral Trainee.

These methods have been applied to nickel and chromium; the room temperature results for nickel compare favorably with X-ray Debye temperatures reported by Simerska (1962) and Goldak (1965). Chromium, however, seems to give a somewhat lower X-ray Debye temperature than has been reported by Ilyina & Kristskaya (1955).

Theory

The basic theory employed in this work was developed by several authors. Our notation is similar to that of James (1954) where a detailed development and references can be found. The relation developed for the scattered X-ray intensity is given by the following expression:

$$\langle I(\bar{S})/\lambda)\rangle = C|f_o|^2 e^{-2M} I_0(\bar{S}/\lambda) + I_2(\bar{S}/\lambda) \qquad (1)$$

where

$$2M = \frac{12 \cdot h^2}{mk\Theta_M}\left\{\frac{F(X)}{X} + \frac{1}{4}\right\}\left(\frac{\sin\theta}{\lambda}\right)^2; \qquad (2)$$

$$F(X) = \frac{1}{X}\int_{\xi=0}^{X} \xi\,(e^{\xi}-1)^{-1} d\xi;\ X = \frac{\Theta_M}{T}; \qquad (3)$$

$$C = (e^2/mc^2)^2 \frac{1+\cos^2 2\theta}{2R^2}; \qquad (4)$$